Applied Thermal Engineering 180 (2020) 115884

Contents lists available at ScienceDirect

Applied Thermal Engineering

journal homepage: www.elsevier.com/locate/apthermeng

Performance of counter flow membrane-based annular pipe liquid desiccant air conditioner

Ertuğrul Cihan[a], Barış Kavasoğullari[a], Hasan Demir[b,*]

[a] Osmaniye Korkut Ata University, Department of Mechanical Engineering, Karacaoglan Campus, 80000 Osmaniye, Turkey
[b] Osmaniye Korkut Ata University, Department of Chemical Engineering, Karacaoglan Campus, 80000 Osmaniye, Turkey

HIGHLIGHTS

- Counter flow membrane-based annular pipe liquid desiccant air conditioner is designed.
- 3D numerical model is developed in COMSOL to investigate system performance.
- Numerical simulation is validated with experimental data.
- Mass transfer correlation is fitted.
- Effects of operation parameters on performance are investigated.

GRAPHICAL ABSTRACT

Experimental rig, flow patterns of the air&solution streams schematic view and numerical simulation of the membrane-based AP_LDAC dehumidification system.

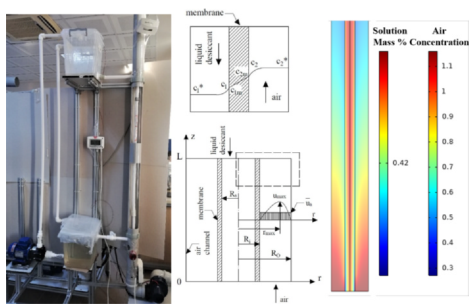

ARTICLE INFO

Keywords:
Semi-permeable membrane
Membrane-based liquid desiccant
Dehumidification
Liquid desiccant
Air conditioner

ABSTRACT

The present study comprises an experimental and numerical simulation of a counter flow membrane-based annular pipe liquid desiccant air conditioner (AP_LDAC) system. The experimental rig was constructed by using DuPont™ Tyvek® Solid as semi-permeable membrane and it has simplier structure compared to other types of membrane-based dehumidifiers. To validate the numerical data, experiments were carried out at different air side Reynolds (*Re*) number. The 3D numerical simulation of counter flows of the AP_LDAC system presented good agreement (R-square: 0.9659) with experimental data, as a result of the validation. Once the reliability of numerical data were verified, the mass transfer coefficient of counterflow obtained by designed system was revealed and optimized numerically by investigating for various aspect ratios, Reynolds (*Re*) and Schmidt (*Sc*) numbers. The derived *Sh* model was predicted over COMSOL *Sh* numbers with error interval from 0.1% to 10%. The effect of air inlet temperatures on temperature, concentration distributions and efficiency of the optimized AP_LDAC system were also investigated. The dehumidification efficiency was found as 99% for the maximum aspect ratio and the lowest *Re* number.

1. Introduction

Nowadays, most of the population spends almost 90% of their time indoors, hence the energy demand to maintain a comfortable living environment constitutes 20–40% of the overall building's energy consumption. Especially in the summertime, at hot and humid climates, most of the consuming energy is used for dehumidification processes. Application of liquid desiccant system integrated to an air conditioning

* Corresponding author.
E-mail addresses: ertugrul.cihan@osmaniye.edu.tr (E. Cihan), bkavasogullari@osmaniye.edu.tr (B. Kavasoğullari), hasandemir@osmaniye.edu.tr (H. Demir).

https://doi.org/10.1016/j.applthermaleng.2020.115884
Received 8 May 2020; Received in revised form 23 July 2020; Accepted 10 August 2020
Available online 14 August 2020
1359-4311/

Nomenclature

A, B, C	Antoine Eqn. constants
c	concentration, mol m^{-3}
c_p	Specific heat, kJ kg^{-1} K^{-1}
d_e	equivalent diameter, m
D	Membrane Diameter, (m)
D_a	Water vapor- air diffusivity, m^2 s^{-1}
D_m	Water vapor-membrane diffusivity, m^2 s^{-1}
D_s	Water vapor-desiccant solution diffusivity, m^2 s^{-1}
h_d	Eq. (19)
k	mass transfer coefficient, m s^{-1}
L	fibre length, m
m	Mass, kg
M_A	Molar mass of water, kg mol^{-1}
N	Mass flux, kg m^{-1} s^{-1}
P	Pressure, kPa
q	Heat flux, W m^{-2}
r	Radial distance, m
R	Radius, m
R_u	Universal gas constant, Pa m^3 mol^{-1} K^{-1}
Re	Reynolds number
S	Cross-sectional area, m^2
Sc	Schmidt number
Sh	Sherwood number
Sh_0	Eq. (23)
T	Absolute temperature, K
u	Velocity, m s^{-1}
z	Longitudinal distance, m
α	Eq. (18a)
β	Eq. (18a)
δ	Membrane thickness, m
η	Efficiency
κ	Eq. (18a)
λ	Thermal conductivity, W m^{-1} K^{-1}
μ	Dynamic viscosity, Pa s
ξ	Mass fraction of solute, kg kg^{-1}
π	Relative pressure
ρ	Density, kg m^{-3}
ϕ	Relative humidity

Subscripts

1,2,3....	State number
a	Air, air channel
A	Eqs. (20)–(22)
c	At the critical point
e	equivalent
i	Inner, inlet
LiCl	Lithium chloride
m	membrane
o	Outer, outlet
s	Solution, solution channel
v	vapor
w	water

Superscript

*	Eqs. (21) and (22)
sat	Saturated

system in populous places (cinemas, mall, conference hall, hospital, etc.) would reduce 25–35% of the consumed electricity since latent heat load can be removed by the proposed system and sensible heat load can be provided by air conditioning system [1]. The liquid desiccant directly contacts with air in the open liquid desiccant system. This provokes carryover of solution droplets through the environment. The use of membrane liquid desiccant system in the air conditioning application has started since porous membrane allows vapor to permeate and a barrier to liquid [2]. Membrane-based liquid desiccant dehumidification systems have started to be used in air conditioning applications to eliminate the abovementioned drawbacks. In the last decade, there have been 94 scientific publications on SCI magazines. This number was only 10 before the year 2011 [3,4].

Three types of designs; tubular, parallel-plate and elliptical stand out in the literature. In the literature survey, there are numerical studies on hollow fiber membrane-based liquid desiccant systems which are at microscale and, hollow fiber simulation is a part of shell and tube membrane desiccant system. Huang et. al., [5] carried out heat and mass transfer analysis in a hollow fiber membrane bundle designed for the liquid desiccant dehumidification system. They used modified PVF (polyvinyl fluoride) as membrane and experimental studies were performed to verify numerical analysis results. They reported that Sherwood and Nusselt numbers were greater at staggered tube arrangement than straight arrangements as a result of the study. Chen et. al., [6] numerically and experimentally analyzed the performance of a novel polymer hollow fiber air dehumidifier. They investigated effects of different operating conditions such as air velocity, solution inlet temperature, solution mass flow rate and solution to air specific humidity ratio on the latent and sensible effectivenesses of the system. They reported that the latent and sensible effectivenesses decreased from 0.58 to 0.14 and 0.74 to 0.08, respectively, when the air velocity was increased from 1.5 to 4.5 m/s. Xiao et al. [7] studied novel internally-cooled plate type membrane-based dehumidifier and they found the cooling COP (Coefficient of performance) of the system in between 0.46 and 0.62. The results also show that, the dehumidification and cooling efficiencies of the novel system varied between 0.2–0.62 and 0.24–0.65 respectively, in different air side flow rates. Chen et al. [8] performed experimental analysis of the parallel-plate type dehumidification system for various operating conditions. They reported that, the dehumidification effectiveness improved by 36.9% when the relative humidity of the inlet air increased from 46% to 70%. Zhang et al. [9] investigated the effect of airflow type in shell and tube membrane contactor. In the study, they found that Nusselt and Sherwood numbers were greater than counter flow in the case of Reynolds number greater than 35, but the air side pressure drop was less in crossflow Huang et al. [10] investigated heat and mass transfer characteristics of a hollow fiber membrane tube bank for various pitch-to-diameter ratios and they conducted experimental analysis to validate the numerical results. As a result of the study, the sweeping air side Sherwood and Nusselt numbers increased with increasing pitch-to-diameter ratios. Bai et al [11] carried out numerical and experimental analysis of a parallel-plate type membrane-based dehumidifier and they focused on effects of operating parameters on the system performance. Results showed that, the system effectiveness significantly influenced by solution-to-air mass ratio and NTU (Number of transfer units). Ouyang and Zhang [12] performed heat and mass transfer analyses of a skewed flow hollow fiber membrane tube bank and they conducted experimental tests to validate the numerical results. They reported that, air and solution side Nusselt and Sherwood numbers greatly increased with air skewed angles for various pitch-to-diameter ratios. Huang and Yang [13] also studied the effect of Reynolds number on heat and mass transfer in membrane-based elliptical dehumidification system. In the system, the increase in the number of Reynolds in the airflow along the elliptical fiber indicated that Nusselt and Sherwood numbers were increased. Zhang [14] used an analytical approach in the analysis of the membrane-based tubular liquid desiccant dehumidification system. In the purposed system, the effect of airflow rate on sensible, latent and total effectiveness and dimensionless parameters such as Lewis number and NTU which determines heat and mass transfer performances. The analytical calculations made were then verified experimentally. As a result of the study, sensible, latent and NTU decreased with air flow rate since Lewis number increased. Abdel-Salam et al. [15] performed an analysis of a membrane-based parallel-plate type liquid desiccant dehumidification system using the TRNSYS programmer. The coefficient of performance of the system was calculated as 0.68 and for a different climate, operating, and design conditions sensible heat ratio of air varied between 0.3 and 0.5. Das and Jain [16] studied the effects of membrane characteristics, contactor design, flow rates, ambient conditions and liquid desiccant concentration on the performance of membrane-based liquid desiccant dehumidification system. As a result of the study, the system performance was determined to be significantly dependent on the membrane characteristics, especially porosity, pore diameter, and membrane thickness.

The performance of the liquid desiccant air conditioner (LDAC) systems mainly depends on properties of the membrane which are permeability of water vapor, pore radius, surface tension leakage of the solution, durability to operating pressure, and durability to operating temperature, etc. [17–19]. Most of the membranes used in LDAC are polymeric materials having a microporous and nonporous structure [20]. The nonporous membrane is produced by woven and non-woven techniques. The membrane used in the current study was DuPont™ Tyvek® Solid which is a non-woven and non-perforated sheet made by spinning high-density polyethylene fibers. Larson [21] designed and tested a rectangular membrane-based run-around energy exchanger (RAEE) for dehumidified air. The DuPont™ Tyvek® and 3M™ Propore™ commercial membranes were used in the RAEE system. The permeability of DuPont™ Tyvek® has twice the water vapor resistance than that of 3M™ Propore™. Moghaddam et al. [22] investigated experimentally the performance of a small scale single panel liquid to air membrane energy exchanger (LAMEE) under the air inlet temperature and humidity ratio between 15–50 °C and 1–28 gw/kgair, respectively, for the supply air velocity range of 1–3 m/s. In small scale single panel LAMEE, GE™ membrane is used. The maximum air and solution side dehumidification effectiveness of the small-scale single panel LAMEE is 91% and 90%, respectively.

In the literature, the main research gap in the membrane-based LDAC system was constructed and/or simulated system were in microscale it is difficult to find the real application and/or real applicable size of.

Literature survey shows that the main research gap in the membrane-based liquid desiccant systems was their dimensions which are mostly in microscale and are not suitable for real case application. The aim of this study was to design, construct and numerically simulate a real application sized counter flow membrane-based annular pipe liquid desiccant air conditioner. The experimental rig of LDAC was setup in metric dimensions and it has simplier and cheaper design which can easily be adapted to air-conditioning systems. The membrane-based LDAC system was designed in the annulus pipe form. The LiCl desiccant solution flows inside the membrane pipe by gravity. Humid air flows against gravity counter flow the desiccant solution outside the membrane pipe and inside the outer pipe. In the light of experimental results, numerical simulation of AP_LDAC system was investigated using the COMSOL Multiphysics programmer. Through the numerical simulation, a liquid–air mass transfer correlation was obtained for the AP_LDAC dehumidification system. Effect of aspect ratio (5, 10, 20,40, 80, and 160), *Re* numbers (25, 100, 400, 800, and 2000), the Schmidt number (0.68, 1.36, 2.20, and 3.40) on the mass transfer correlation were investigated.

2. Experimental apparatus and test procedures

Fig. 1 illustrates the photograph and schematic view of the designed and constructed AP_LDAC. The desiccant solution was pumped from the bottom reservoir to the upper reservoir by Gemmecotti HTM 4 PP magnetic driven pump. The LiCl solution flows inside the Tyvek® Solid pipe having a 20 mm inner diameter with gravity. Air was humidified to obtain maximum efficiency of the system and comparable results independent from the relative humidity of the air. Humid air flows as counter flow according to desiccant solution inside PVC pipe having 72 mm inner diameter. The air velocity was adjusted by manipulating rpm of air fan (TMC centrifugal fan 24 V, 3679 L/min). Inlet and outlet relative humidity and temperatures of air were measured by VAISALA

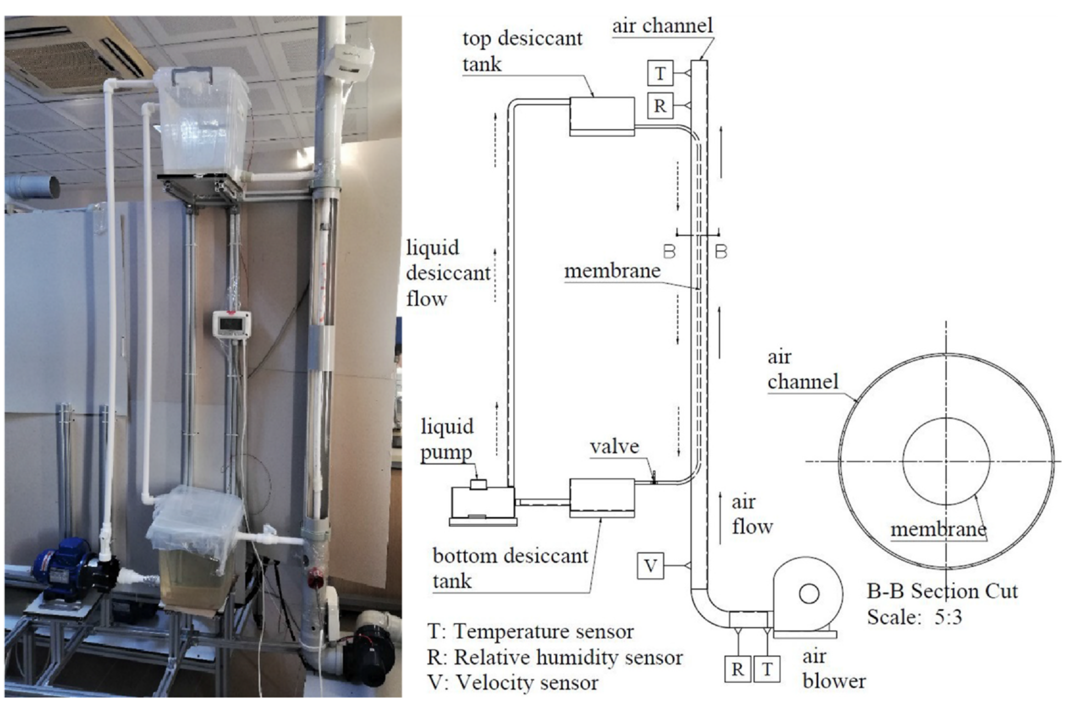

Fig. 1. Experimental rig and schematic view of the membrane-based AP_LDAC dehumidification system.

HMT120. Relative humidity and temperature were measured with ± %1.5 and ± 0.2 °C accuracy, respectively. The velocity of air was measured using a hot wire KIMO-CTV210 sensor (0–30 m/s) with ± %0.3 accuracy. The temperature of desiccant was measured by K type thermocouples from the inlet and outlet of the membrane pipe. Heat generation on the outer surface of membrane pipe during absorption of water vapor was measured by Testo 881 thermal camera with ± 2 °C precision. The procedures followed in the experiments are listed below:

- The air fan was adjusted to the air velocity corresponding to the *Re* number to be tested. The humidifier unit was activated to provide humid air to the system.
- At the beginning of the experiments, only humid air was passed through the system for about 10 min to stabilize the velocity and relative humidity of the air flow.
- After air flow was stabilized, liquid pump was activated to circulate the liquid desiccant. In order to prevent the desiccant from overflowing from the top desiccant tank, the liquid pump was operated at 26 Hz frequency value.
- During the experiments, air velocity, inlet/outlet temperatures and relative humidities were measured in every 10 s with the help of SCADA software.
- After 40–50 min of experiment, the measured data were saved on the computer and the system is turned off.

3. Mathematical and numerical model

The liquid to air dehumidification process in the membrane liquid desiccant system is based on water vapor diffusion from moist air through the desiccant solution by passing membrane as shown in Fig. 1. The following assumptions were made for modeling the 3D AP_LDAC system in the dehumidification of air.

- Steady-state
- Momentum, heat, and moisture transfers occur in the radial (r), angular (θ), and longitudinal (z) directions.
- The geometry of flow channels is identical.
- Heat and moisture transfers between the system and the surroundings are negligible
- Desiccant and air flows were assumed as hydrodynamically laminar fully developed.
- Phase change energy from the evaporation/condensation of water vapor at the liquid-membrane interface is all transferred from/to the liquid

In Fig. 2, the flow patterns of the air and solution streams are illustrated. As it seems in Fig. 2, the air flows at the annular channel in z-direction while the solution flows at a circular channel counter currently in the negative z-direction.

The steady-state momentum, energy and moisture transfer equations for the airstream are defined as followings [23]:

$$\mu_a\left[\frac{1}{r}\frac{\partial}{\partial r}\left(r\frac{\partial u_a}{\partial r}\right)+\frac{1}{r^2}\frac{\partial^2 u_a}{\partial\theta^2}+\frac{\partial^2 u_a}{\partial z^2}\right]=-\frac{dP_a}{dz} \tag{1}$$

$$\lambda_a\left[\frac{1}{r}\frac{\partial}{\partial r}\left(r\frac{\partial T}{\partial r}\right)+\frac{1}{r^2}\frac{\partial^2 T}{\partial\theta^2}+\frac{\partial^2 T}{\partial z^2}\right]=\rho_a c_{p,a}u_a\left(\frac{\partial T}{\partial z}\right) \tag{2}$$

$$D_a\left[\frac{1}{r}\frac{\partial}{\partial r}\left(r\frac{\partial c}{\partial r}\right)+\frac{1}{r^2}\frac{\partial^2 c}{\partial\theta^2}+\frac{\partial^2 c}{\partial z^2}\right]=u_a\left(\frac{\partial c}{\partial z}\right) \tag{3}$$

For the membrane side, no need to assign the momentum equation since there is no flow. Energy and moisture transfer equations for the membrane were expressed by Eq. (4) and Eq. (5) [23]:

$$\lambda_m\left[\frac{1}{r}\frac{\partial}{\partial r}\left(r\frac{\partial T}{\partial r}\right)+\frac{1}{r^2}\frac{\partial^2 T}{\partial\theta^2}+\frac{\partial^2 T}{\partial z^2}\right]=0 \tag{4}$$

$$D_m\left[\frac{1}{r}\frac{\partial}{\partial r}\left(r\frac{\partial c}{\partial r}\right)+\frac{1}{r^2}\frac{\partial^2 c}{\partial\theta^2}+\frac{\partial^2 c}{\partial z^2}\right]=0 \tag{5}$$

Momentum, heat and moisture transfer through the solution are described in the following equations [23]:

$$\mu_s\left[\frac{1}{r}\frac{\partial}{\partial r}\left(r\frac{\partial u_s}{\partial r}\right)+\frac{1}{r^2}\frac{\partial^2 u_s}{\partial\theta^2}+\frac{\partial^2 u_s}{\partial z^2}\right]=-\frac{dP_s}{dz} \tag{6}$$

$$\lambda_s\left[\frac{1}{r}\frac{\partial}{\partial r}\left(r\frac{\partial T}{\partial r}\right)+\frac{1}{r^2}\frac{\partial^2 T}{\partial\theta^2}+\frac{\partial^2 T}{\partial z^2}\right]=\rho_s c_{p,s}u_s\left(\frac{\partial T}{\partial z}\right) \tag{7}$$

$$D_s\left[\frac{1}{r}\frac{\partial}{\partial r}\left(r\frac{\partial c}{\partial r}\right)+\frac{1}{r^2}\frac{\partial^2 c}{\partial\theta^2}+\frac{\partial^2 c}{\partial z^2}\right]=u_s\left(\frac{\partial c}{\partial z}\right) \tag{8}$$

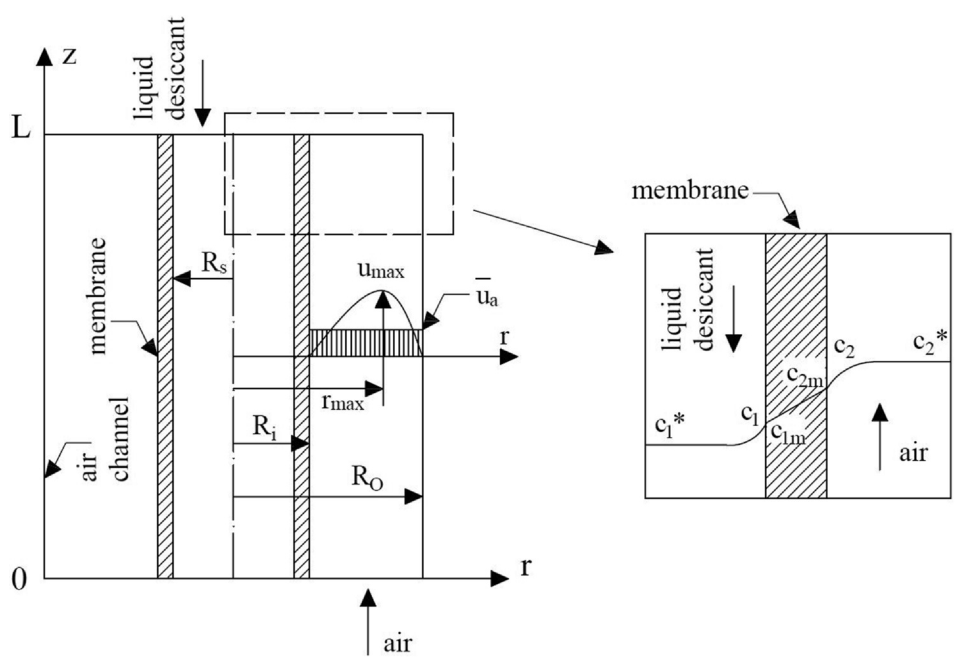

Fig. 2. The flow patterns of the air and the solution streams in the AP_LDAC system.

Table 1
Vapor pressure constants for LiCl solution.

Constants	LiCl-water
π_0	0.28
π_1	4.3
π_2	0.6
π_3	0.21
π_4	5.1
π_5	0.49
π_6	0.362
π_7	−4.75
π_8	−0.4
π_9	0.03

Table 2
Flow chart for the numerical procedure.

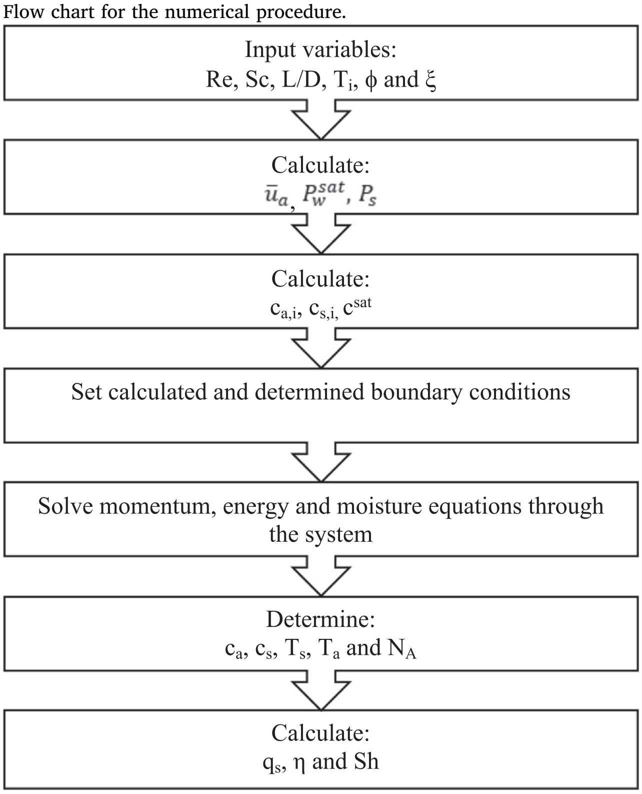

Table 3
The average velocity of the air stream corresponding to *Re* numbers.

Re	25	100	400	800	2000
$\bar{u}_a$**(m/s)**	0.006	0.025	0.1	0.2	0.49

The Reynolds number of the air stream is defined in Eq. (9):

$$Re_a = \frac{\rho_a \bar{u}_a d_e}{\mu_a} \tag{9a}$$

$$d_e = \sqrt{\frac{4S_a}{\pi}} \tag{9b}$$

$$S_a = \pi(R_o^2 - R_i^2) \tag{9c}$$

The Schmidt number of the air stream is:

$$Sc = \frac{\mu_a}{\rho_a D_a} \tag{10}$$

The Sherwood number of the air stream is defined in Eq. (11):

Table 4
Calculation parameters used in numerical analysis.

Parameters	Symbol	Unit	Value
Water vapor diffusivity of the membrane	D_m	m^2/s	1.35×10^{-6}
Water vapor diffusivity of the air [25]	D_a	m^2/s	2.5×10^{-5}
Water vapor mass transfer coefficient of the air [26]	k_a	m/s	2.5×10^{-2}
Water vapor mass transfer coefficient of the solution [24]	k_s	m/s	4.204×10^{-3}
Diameter of the membrane tube	D	mm	20
Length of the tube	L	mm	L/D*D
Ratio of the membrane tube diameter to the air channel diameter	D/D_o	–	0.28
Membrane thickness	δ	mm	0.25
Initial temperature of the air and solution streams	T_i	K	298
Antoine equation constant	A		16.3872
Antoine equation constant	B		3885.7
Antoine equation constant	C		230.15

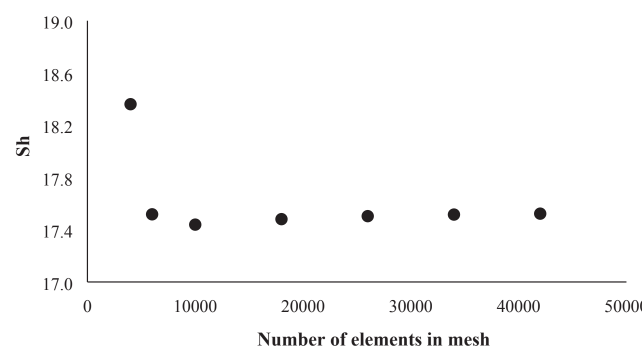

Fig. 3. Grid sensitivity analysis for L/D = 10.

Table 5
Precisions of used device in the system.

Device	Parameter	Measurement Range	Accuracy
Vaisala HMT120	Relative humidity	0–100	± 1.5%
	Temperature	−40 to +80 °C	± 0.2 °C
Kimo-CTV210	Gas flow	0–30 m/s	± 0.3%

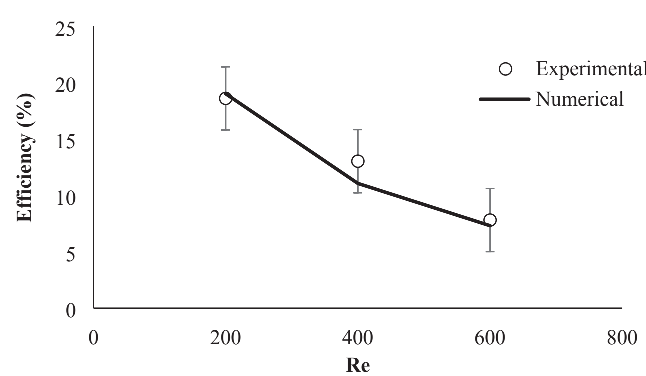

Fig. 4. Comparison of efficiency values of COMSOL (lines) and experimental study (dots).

$$Sh = \frac{k_a d_e}{D_a} \tag{11}$$

The dehumidification efficiency of the system is defined by

$$\eta(\%) = 100\frac{(C_{a,i} - C_{a,o})}{(C_{a,i} - C^{sat})} \tag{12}$$

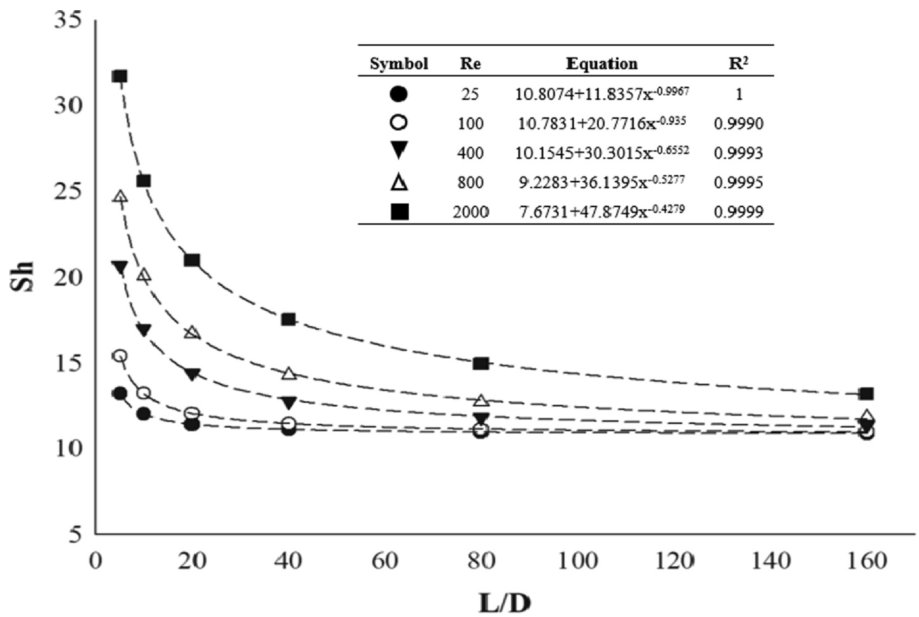

Fig. 5. Variation of Sherwood numbers against aspect ratio and fitted equations.

where $c_{a,i}$ and $c_{a,o}$ are the inlet and outlet concentration (mol m^{-3}) of the air respectively. c^{sat} is the water vapor concentration (mol m^{-3}) of the desiccant solution in equilibrium with air.

3.1. Boundary conditions

In the AP_LDAC system, flow patterns of the air and the solution are illustrated in Fig. 2. According to the Fig. 2, $u_a = 0$ and $u_s = 0$ at the walls due to no-slip condition.

At the airside, inlet conditions for the temperature and concentration are given in below Eqs.:

$$z = 0, \quad T_a = T_i \tag{13a}$$

$$z = 0, \quad c_a = c_{a,i} \tag{13b}$$

Here, T_i is the initial prescribed temperature and $c_{a,i}$ is defined in Eq. (14):

$$c_{a,i} = \frac{\varnothing P_w^{sat}}{R_u T} \tag{14}$$

P_w^{sat} is the saturation pressure (kPa) of the water vapor in the air and can be calculated by using Antonie equation as following:

$$lnP_w^{sat} = A - \frac{B}{T + C} \tag{15}$$

where the unit of T is °C. At the air outlet (z = L), $\nabla T_a = 0$ and $\nabla c_a = 0$. The inlet conditions for the solution side are given by

$$z = L, \quad T_s = T_i \tag{16a}$$

$$z = L, \quad c_s = c_{s,i} \tag{16b}$$

where $c_{s,i}$ indicates the water vapor concentration (mol m^{-3}) in the desiccant solution defined in Eq. (17):

$$c_{s,i} = \frac{P_s}{R_u T} \tag{17}$$

At the solution outlet (z = 0), $\nabla T_s = 0$ and $\nabla c_s = 0$. In Eq. (17), P_s denotes the water vapor pressure of the LiCl solution (kPa) which must be lower than the water vapor pressure of the air to accomplish the dehumidification process. P_s may be found by Eq. (18), purposed by Conde [24]:

$$\frac{P_s}{P_w^{sat}} = \alpha\left(\beta + \kappa\frac{T}{647.096}\right) \tag{18a}$$

$$\beta = 2 - \left[1 + \left(\frac{\xi}{\pi_0}\right)^{\pi_1}\right]^{\pi_2} \tag{18b}$$

$$\kappa = \left[1 + \left(\frac{\xi}{\pi_3}\right)^{\pi_4}\right]^{\pi_5} - 1 \tag{18c}$$

$$\alpha = 1 - \left[1 + \left(\frac{\xi}{\pi_6}\right)^{\pi_7}\right]^{\pi_8} - \pi_9 e^{\frac{-(\xi-0.1)^2}{0.005}} \tag{18d}$$

$$\xi = \frac{m_{LiCl}}{m_{LiCl} + m_w + \Delta m_v} \tag{18e}$$

In the previous eq., π_i is the vapor pressure constants for the LiCl solution and are given in Table 1.

In dehumidification, absorption of water vapor by desiccant is an exothermic reaction that causes heat release by the desiccant solution. The released heat may be defined by

$$q_s = N_A M_A h_d \tag{19}$$

where h_d is the differential enthalpy of dilution value (~3.10^6 J kg^{-1}) at the corresponding temperature of the LiCl solution which was taken from Conde [24]. M_A and N_A are the molar weight (kg mol^{-1}) of the water vapor and mass flux through the membrane (mol m^{-2} s^{-1}), respectively. N_A is defined by below equations:

$$N_A = \frac{D_m}{\delta}(c_{2m} - c_{1m}) \tag{20}$$

$$N_A = k_a(c_2^* - c_2) \tag{21}$$

$$N_A = k_s(c_1 - c_1^*) \tag{22}$$

Eq. (20) represents the mass transfer boundary condition through the membrane and is equal to mass transfer flux at airside (Eq. (21)) and mass transfer flux at the solution side (Eq. (22)). Since the membrane has a thin structure, Fick's law may be used to describe water vapor transfer through the membrane as in Eq. (20). In previous equations, c_{1m} and c_{2m} are the concentrations of solution-membrane and membrane-air interfaces which assumed to approach the c_1 and c_2 concentrations, due to the thin structure of the membrane. c_1* and c_2* are the bulk concentrations of the solution and air streams, respectively.

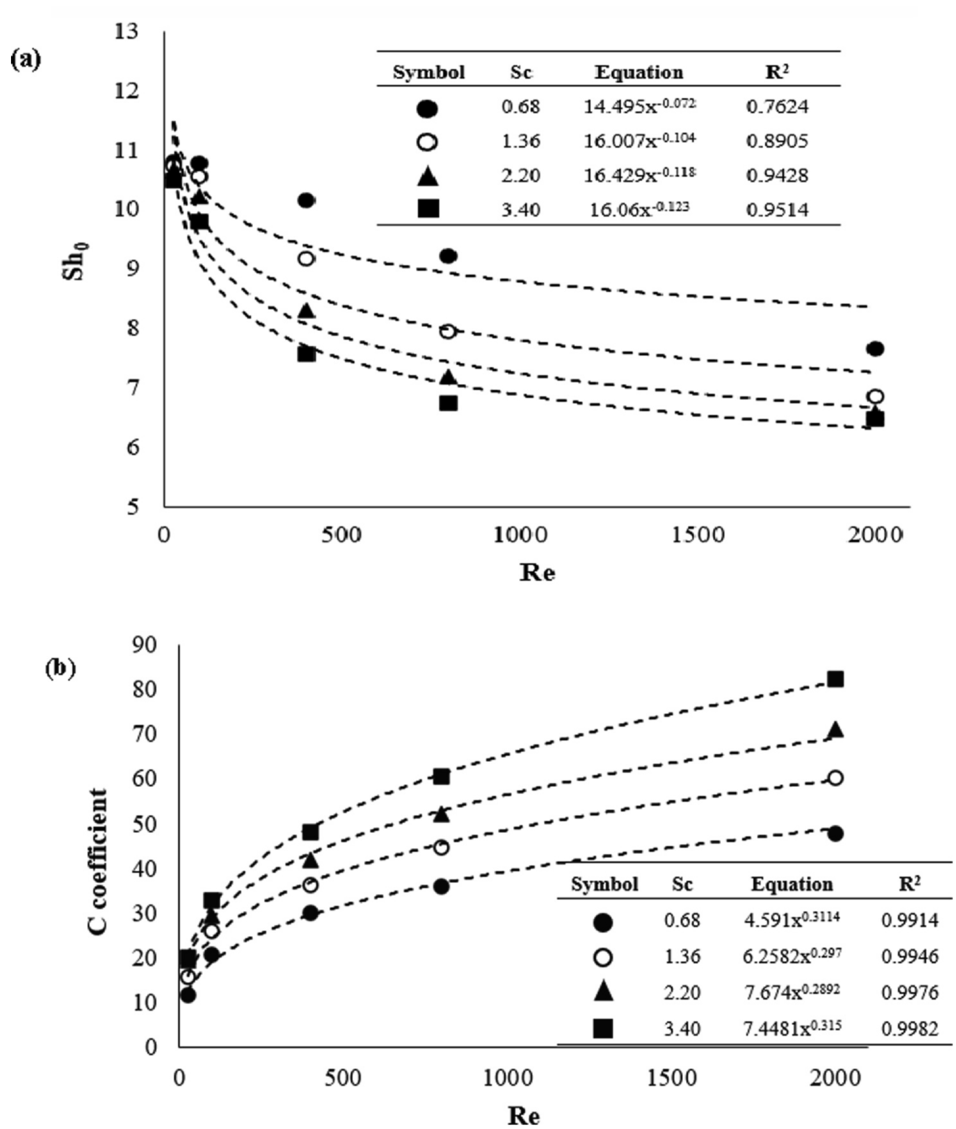

Fig. 6. Variations of a) Sh_0 and b) C coefficients against *Re* numbers.

3.2. Solution procedure

In the numerical analysis, the 3D model was built in the COMSOL Multiphysics according to the experimental shape and dimensions of the AP_LDAC system. The numerical solution procedure is shown in Table 2.

In the calculations, mainly, *Re*, L/D, and *Sc* numbers were specified as input variables to determine the effects of the flow velocity, geometry and mass diffusivity on the mass transfer performance of the system. To analyze the system in laminar flow, 25, 100, 400, 800 and 2000 *Re* numbers were selected for the air stream. The average velocity values corresponding to the *Re* numbers are given in Table 3. Aspect ratios were varied by 5, 10, 20, 40, 80 and 160 in different *Sc* numbers including 0.68, 1.36, 2.2 and 3.4. The other calculation parameters were listed in Table 4.

In the constructed model, four COMSOL modules were used to solve momentum, heat and mass transfer equations. In the Laminar Flow module, the fully developed flow was selected and the average velocity values in Table 2 were given as inlet velocity for the air stream. To calculate the heat released by the desiccant during the dehumidification process, Heat Transfer in Fluids module was used. Moisture transfer equations of the air and the membrane were solved by Transport in Diluted Species module. Transport in Concentrated Species was used to solve the moisture transfer equation through the desiccant solution.

In the COMSOL model, an extremely fine level of mesh element size was applied to the geometry which varied from 5000 to 160,000 depending on aspect ratios. The grid independence test of the calculated *Sh* number is illustrated in Fig. 3 at a specific aspect ratio value. As is seen from Fig. 3, after 15,000 mesh elements, the differentiation in *Sh* number can be negligible.

4. Validation of the model

In order to validate the numerical solution experimentally, some parameters in the numerical solution were changed to be the same as the experimental setup. The length of the tube (L) was set at 740 mm and 200, 400 and 600 *Re* numbers were used to find air velocity. The other parameters were taken from table 4 to carry out calculations. The uncerainity analysis of experimental efficiency of dehumidification was evaluated by equation (23). Table 5 illustrates types of sensors and their accuracy.

$$\frac{\delta\eta}{\eta} = \sqrt{\left(\frac{\delta\omega_g}{\omega_g}\right)^2 + \left(\frac{\delta\omega_c}{\omega_c}\right)^2 + \left(\frac{\delta\omega^{sat}}{\omega^{sat}}\right)^2} \tag{23}$$

Uncertainty analysis was performed using EES programme which

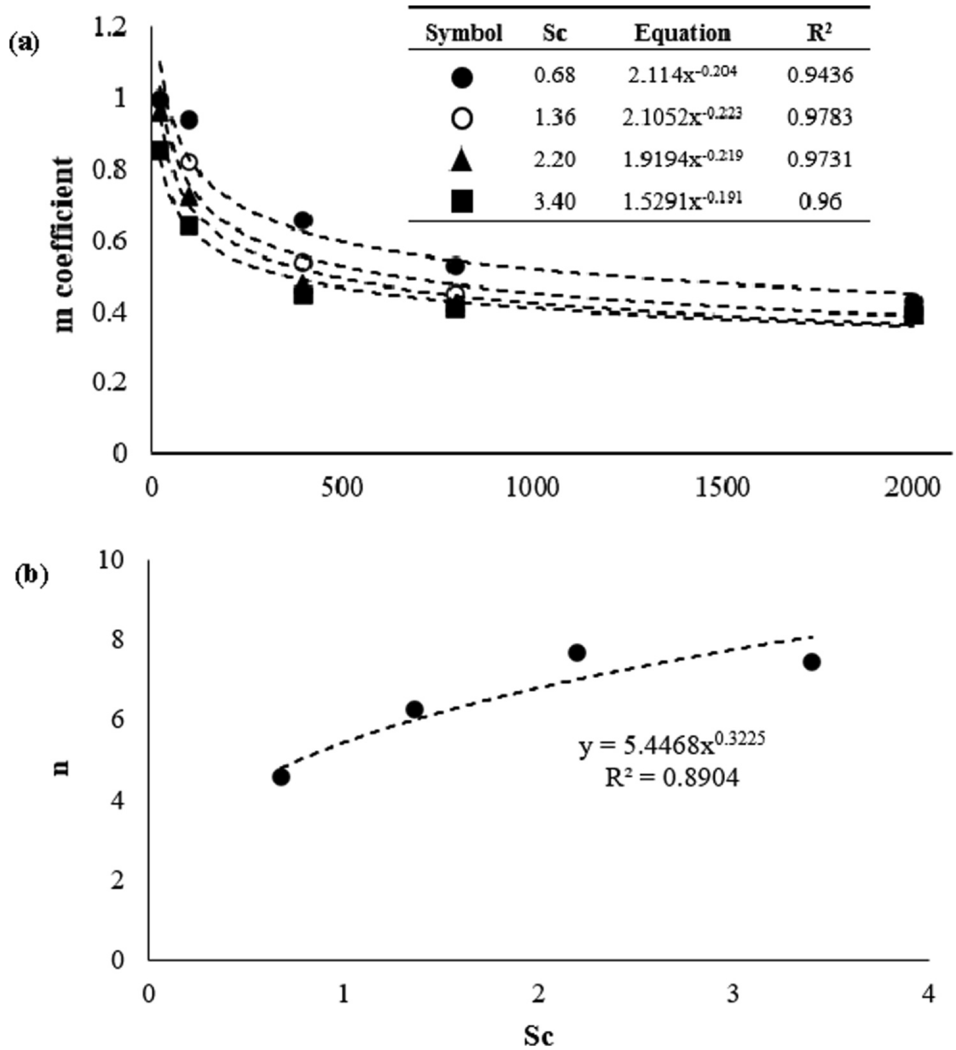

Fig. 7. Variations of a) m power of *Re* and b) n power of *Sc*.

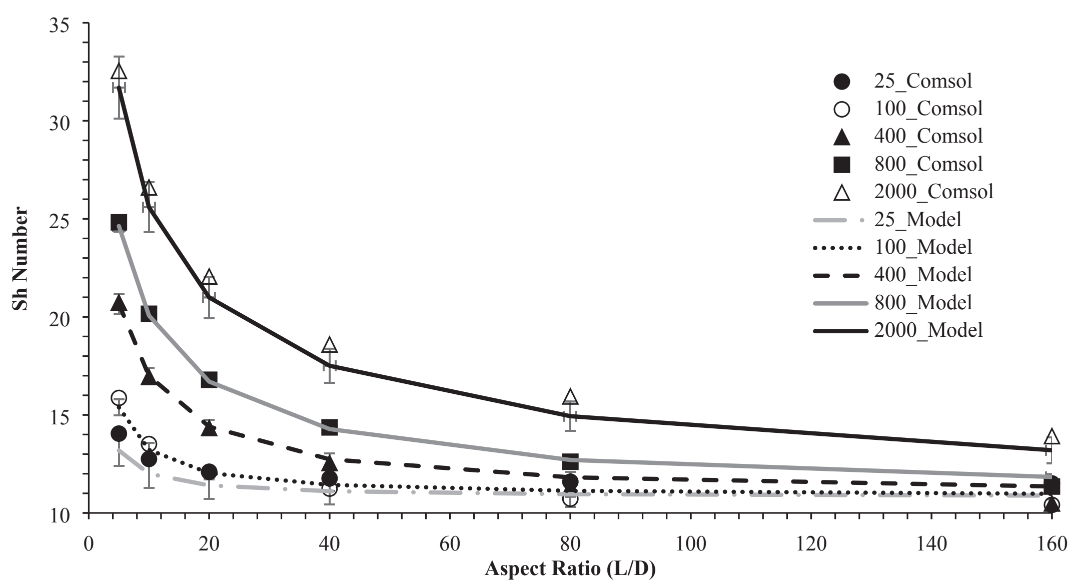

Fig. 8. Comparison of *Sh* number obtained from COMSOL and derived model and error percentage.

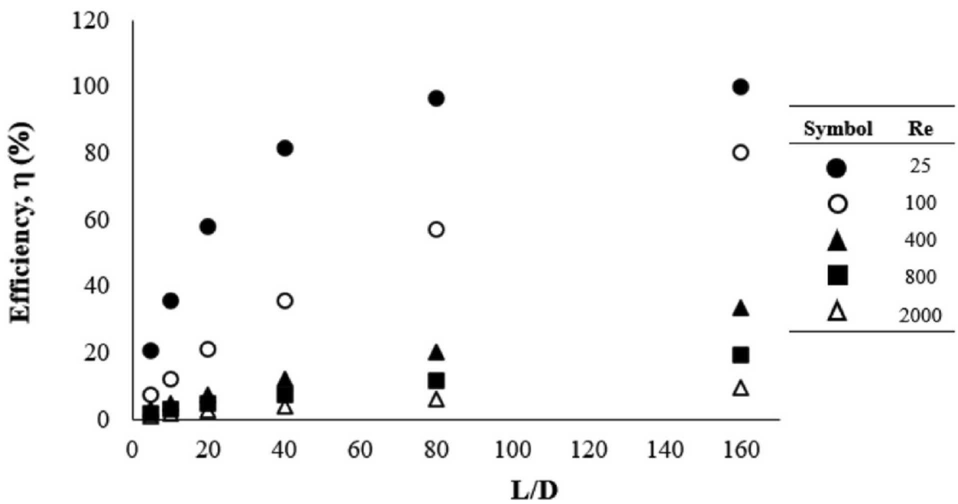

Fig. 9. Dehumidification performance of AP_LDAC system against aspect ratio for different *Re* numbers.

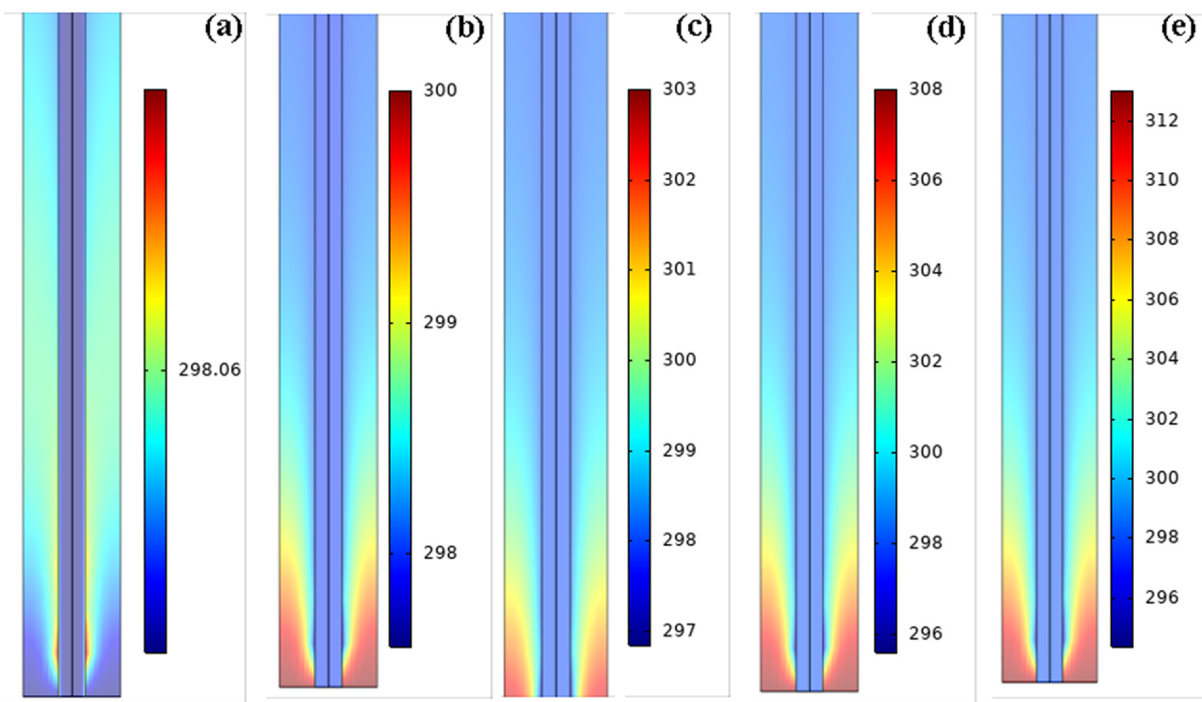

Fig. 10. Effect of air inlet temperature a) 298 K, b) 300 K, c) 303 K, d) 308 K, and e) 313 K on AP_LDAC system.

uses root sum square technique. According to this analysis, uncertainty levels were determined as ± 2.8 for dehumidification efficiency. The measurement errors were reflected to the calculated performance indicators reasonably.

Fig. 4 illustrates the comparison of efficiency values of COMSOL and experimental study. The numerical and experimental lines present good agreement with 0.9659 regression constant. As a result of validation, it can obviously be said that the numerical simulation constituted in COMSOL Multiphysics represented the mass and heat transfer problem of the AP_LDAC system accurately.

5. Results and discussions

The mass transfer coefficient which is Sherwood number was correlated to the Reynolds number (25, 100, 400, 800, and 2000), the Schmidt number (0.68, 1.36, 2.20, and 3.40) and aspect ratio of the annular tube (5, 10, 20, 40, 80, and 160) for AP_LDAC system. Then Eq. (24) presented a general form of Sherwood number. The constants are given in the Eq. (24) were defined by a numerical simulation study in given numbers and their variations.

$$Sh = Sh_0 + CRe^m Sc^n \tag{24}$$

Fig. 5 illustrates the Sherwood number variations according to the aspect ratio of the annular pipe which is a physical factor that can influence the mass transfer rate in a desiccant system. It should be kept in mind that the flows of air and desiccant inside the membrane were counter current. The heat evolution during water vapor absorption by desiccant is counted in a numerical simulation study. The Sherwood number was very high at the low aspect ratio as seen in Fig. 5. The high *Sh* numbers may be as result of the undeveloped and low thickness of the concentration boundary layer [3]. Increment of aspect ratio causes decrease in the Sherwood number. The small tables in Fig. 5 indicated that the *Re* numbers also affected the mass transfer in the system in accordance with the general form of *Sh* number equation.

Fig. 6 shows the change of Sh_0 and C constants against *Re* numbers.

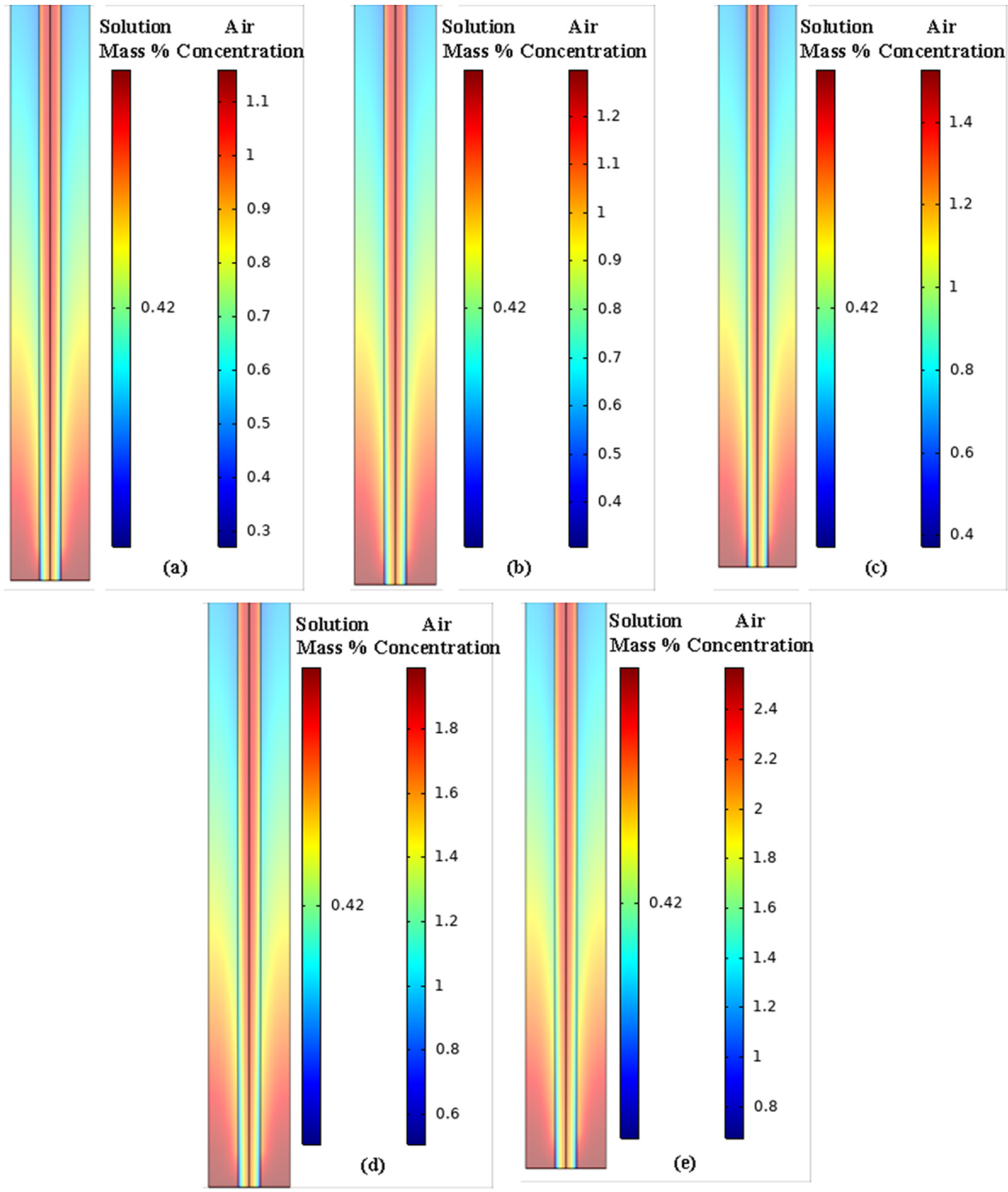

Fig. 11. Variation of solution mass fraction and air concentration against to air inlet temperature a) 298 K, b) 300 K, c) 303 K, d) 308 K, and e) 313 K.

As seen in Fig. 6a, the Sh_0 decreases with increasing *Re* numbers. The increment of *Re* numbers denoted the increment of air velocity as shown in Table 2. The increment of air velocity causes to reduce contact time of air and desiccant and presence of the membrane should be kept in mind that is an additional mass transfer resistance between humid air and desiccant solution. The small table in Fig. 4a indicates that the Sh_0 number was independent of *Sc* number. The C coefficient increases with increasing *Re* numbers as shown in Fig. 6b. The C coefficient was also independent of *Sc* number.

Fig. 7 depicts the behaviors of powers of *Re* and *Sc* numbers in Eq. (24). The m and n powers were defined with fitted lines. Eventually, the *Sh* number was identified as a function of *Re*, *Sc*, and aspect ratio in Eq. (24).

$$Sh = 15.75Re^{-0.1} + 5.45Re^{0.3}\left(\frac{D}{L}\right)^{a} Sc^{0.323}; \quad a = 1.917Re^{-0.21} \tag{25}$$

The derived *Sh* model was predicted over COMSOL *Sh* numbers with error interval from 0.1% to 10%. Fig. 8 illustrates the comparison of *Sh* number obtained from COMSOL and derived *Sh* model and error percentage. As seen in Fig. 8, most of the error bars cannot be noticed due to a very low error of percentage. This phenomenon proves that the derived *Sh* model comprised all studied conditions very well which are aspect ratio from 10 to 160, *Re* numbers from 25 to 2000 and *Sc* numbers from 0.68 to 3.4.

Fig. 9 represents the variation of dehumidification performance of the AP_LDAC system against aspect ratio for different *Re* numbers. An increment of aspect ratio increased the dehumidification efficiency of the AP_LDAC system for all *Re* numbers since the contact time was increased with the extension of the length of the pipe. The increment of *Re* numbers caused to decrease in the dehumidification efficiency of the AP_LDAC system. In this case, the increment of *Re* number was a result of the increment of air velocity causing reduce contact time of air and desiccant solution as well as restrict to mass transfer rate. Das and Jain [16] reported that the dehumidification efficiency varied between 98 and 30% for different airflow rates in their work. Abdel-Salam et al. [27] obtained up to 50% latent effectiveness with the LAMEE system at specific operating conditions. Fakharnezhad and Keshavarz [28] achieved approximately 99% dehumidification efficiency with a hollow fiber membrane module at low air and high solution flow rates. Huang et al. [29] obtained 80% dehumidification efficiency with a parallel-plate type membrane-based dehumidifier.

The maximum efficiency was observed for 25 of *Re*, 0.68 *Sc*, and the aspect ratio as 80. Effect of air inlet temperature on temperature distribution on desiccant and air sides, the efficiency of AP_LDAC system and mass fraction and concentration distribution of air. Fig. 10 illustrates the effect of air inlet temperatures (298, 300, 303, 308, and 313 K) on temperature distribution on the desiccant and airside of the AP_LDAC system. The temperature distribution, especially on the air side, directly was affected by inlet air temperature as expected. The temperature of the desiccant solution was kept constant during the change of inlet air temperature. Increment of air inlet temperature causes to increase in the distribution temperature on the airside of AP_LDAC. Due to energy loss, air inlet temperature started to decrease along to the annular pipe. However, around 0.5 m away from the inlet of the annular pipe, the distribution of air temperature was homogenized. For that reason, only 0.5 m of the annular pipe was shown in Fig. 10. The efficiency of the AP_LDAC system was influenced by the inlet air temperature. Efficiencies decrease with increasing inlet air temperature. At 298 K inlet air temperature, the efficiency was calculated as 96.7% as shown in Fig. 9. The efficiencies for higher temperatures were 93.4% at 300 K, 89.3% at 303 K, 84.3% at 308 K, and 80.6% at 313 K. Abdel-Salam and Simonson [30] reported that a 12 °C increase in the air inlet temperature caused a decrease in the dehumidification efficiency by approximately 10%. Ge et al. [31] also investigated the effect of air temperature on latent effectiveness and a 5–10% decrease was observed ineffectiveness when the temperature increased by 10 °C.

Fig. 11 represents the variation of solution mass fraction and air concentration against air inlet temperature. The relative humidity was kept as 0.9 for the effect of the inlet air temperature study case. For that reason, the increment of inlet air temperature caused to increase air humidity concentration distribution inside the annular pipe. In a word, the increment of the amount of humidity of air due to the increment of air inlet temperature caused to reduce the efficiency of the AP_LDAC system. When the Eq. (12) was examined, the increment of air inlet temperature caused to increase the denominator of Eq. (12) and efficiencies decreased inherently.

6. Conclusions

The experimental and 3D numerical simulation of the counterflow annular pipe liquid desiccant air conditioner system was successfully investigated. The 3D numerical simulation was validated with 0.9659 regression constant. On the contrary of literature, this study includes real dimensioned experimental rig and various air velocities that can be operated on real applications.

- The general Sherwood mass transfer correlation model was obtained as Eq. (24) with considering aspect ratio (5, 10, 20, 40, 80, and 160), *Re* numbers (25, 100, 400, 800, and 2000), and the Schmidt number (0.68, 1.36, 2.20, and 3.40).
- The derived *Sh* model (Eq. (25)) was predicted over COMSOL *Sh* numbers with an error interval from 0.1% to 10%.
- The increment of *Re* number as well as air velocity caused to decrease drastically dehumidification efficiency of AP_LDAC system.
- The effect of air inlet temperature on the optimized AP_LDAC system was also investigated successfully.
- Efficiencies decrease with increasing inlet air temperature. At 298 K inlet air temperature, the efficiency was calculated as 96.7%. The efficiencies for higher temperatures were found at 93.4% at 300 K, 89.3% at 303 K, 84.3% at 308 K, and 80.6% at 313 K.

Declaration of Competing Interest

The authors declare that they have no known competing financial interests or personal relationships that could have appeared to influence the work reported in this paper.

Acknowledgment

The authors would like to acknowledge OKÜBAP for the financial support of this study (project no: OKÜBAP-2018-PT3-013).

References

[1] Y.S. Ahmed, P. Gandhidasan, A.A. Al-Farayedhi, Thermodynamic analysis of liquid desiccants, Sol. Energy 62 (1998) 11–18, https://doi.org/10.1016/S0038-092X(97)00087-X.
[2] E. Cihan, B. Kavasoğulları, H. Demir, Enhancement of performance of open liquid desiccant system with surface additive, Renew. Energy 114 (2017) 1101–1112, https://doi.org/10.1016/j.renene.2017.08.002.
[3] E. Cihan, B. Kavasoğulları, H. Demir, Mass transfer correlation for tubular membrane-based liquid desiccant air- conditioning system, Arabian J. Sci. Eng. 45 (2020) 519–529, https://doi.org/10.1007/s13369-019-04242-6.
[4] C. Isetti, E. Nannei, A. Magrini, On the application of a membrane air-liquid contactor for air dehumidification, Energy Build. 25 (1997) 185–193, https://doi.org/10.1016/S0378-7788(96)00993-0.
[5] S.M. Huang, L.Z. Zhang, L.X. Pei, Transport phenomena in a cross-flow hollow fibre membrane bundle used for liquid desiccant air dehumidification, Indoor Built Environ. 22 (2013) 559–574, https://doi.org/10.1177/1420326X12452881.
[6] X. Chen, N. Zhang, Y. Su, D. Aydin, H. Zheng, H. Bai, A. Georgakis, H. Jarimi, S. Riffat, Performance analysis and design implementation of a novel polymer hollow fiber liquid desiccant dehumidifier with aqueous potassium formate, Therm. Sci. Eng. Prog. 13 (2019) 100366, , https://doi.org/10.1016/j.tsep.2019.100366.
[7] L. Xiao, M. Yang, W.Z. Yuan, S.M. Huang, Performance characteristics of a novel internally-cooled plate membrane liquid desiccant air dehumidification system, Appl. Therm. Eng. 172 (2020) 115193, , https://doi.org/10.1016/j.applthermaleng.2020.115193.
[8] Z. Chen, J. Zhu, H. Bai, Y. Yan, L. Zhang, Experimental study of a membrane based dehumidification cooling system, Appl. Therm. Eng. 115 (2017) 1315–1321, https://doi.org/10.1016/j.applthermaleng.2016.10.153.
[9] L.Z. Zhang, S.M. Huang, L.X. Pei, Conjugate heat and mass transfer in a cross-flow hollow fiber membrane contactor for liquid desiccant air dehumidification, Int. J. Heat Mass Transf. 55 (2012) 8061–8072, https://doi.org/10.1016/j.ijheatmasstransfer.2012.08.041.
[10] S.M. Huang, M. Yang, J. Tu, Y. Shao, Y. Zuo, Sweeping air membrane distillation: Conjugate heat and mass transfer in a hollow fiber membrane tube bank with an in-line arrengement, Int. J. Heat Mass Transf. 108 (2017) 2191–2197, https://doi.org/10.1016/j.ijheatmasstransfer.2017.01.088.
[11] H. Bai, J. Zhu, Z. Chen, J. Chu, Parametric analysis of a cross-flow membrane-based parallel-plate liquid desiccant dehumidification system: Numerical and experimental data, Energy Build. 158 (2018) 494–508, https://doi.org/10.1016/j.enbuild.2017.10.018.
[12] Y.W. Ouyang, L.Z. Zhang, Conjugate heat and mass transfer in a skewed flow hollow fiber membrane bank used for liquid desiccant air dehumidification, Int. J. Heat Mass Transf. 93 (2016) 23–40, https://doi.org/10.1016/j.ijheatmasstransfer.2015.09.009.
[13] S.M. Huang, M. Yang, Heat and mass transfer enhancement in a cross-flow elliptical hollow fiber membrane contactor used for liquid desiccant air dehumidification, J. Memb. Sci. 449 (2014) 184–192, https://doi.org/10.1016/j.memsci.2013.08.033.
[14] L. Zhang, An analytical solution to heat and mass transfer in hollow fiber membrane contactors for liquid desiccant air dehumidification, ASME J. Heat Transf. 113 (2011) 1–8, https://doi.org/10.1115/1.4003900.
[15] A.H. Abdel-Salam, G. Ge, C.J. Simonson, Performance analysis of a membrane liquid desiccant air-conditioning system, Energy Build. 62 (2013) 559–569, https://doi.org/10.1016/j.enbuild.2013.03.028.
[16] R.S. Das, S. Jain, Performance characteristics of cross-flow membrane contactors for liquid desiccant systems, App. Energy 141 (2015) 1–11, https://doi.org/10.1016/j.enbuild.2013.03.028.
[17] S.M. Huang, L.Z. Zhang, Researches and trends in membrane-based liquid desiccant air dehumidification, Renew. Sustain. Energy Rev. 23 (2013) 425–440, https://doi.org/10.1016/j.rser.2013.08.005.
[18] T.D. Bui, F. Chen, A. Nida, K.J. Chua, K.C. Ng, Experimental and modeling analysis

of membrane-based air dehumidification, Sep. Purif. Technol. 144 (2015) 114–122, https://doi.org/10.1016/j.seppur.2015.02.019.

[19] X. Liu, M. Qu, X. Liu, L. Wang, Membrane-based liquid desiccant air dehumidification: a comprehensive review on materials, components, systems and performances, Renew. Sustain. Energy Rev. 110 (2019) 444–466, https://doi.org/10.1016/j.rser.2019.04.018.

[20] D.I. Petukhov, A.A. Eliseev, A.A. Poyarkov, A.V. Lukashin, Porous polypropylene membrane contactors for dehumidification of gases, Nanosyst.: Phys. Chem. Math. 8 (6) (2017) 798–803, https://doi.org/10.17586/22208054201786798803.

[21] M.D. Larson, The performance of membranes in a newly proposed run-around heat and moisture exchanger, MSci Thesis, Department of Mechanical Engineering at University of Saskatchewan, December, 2006.

[22] D.G. Moghaddam, P. LePoudre, G. Ge, R.W. Besant, C.J. Simonson, Small-scale single-panel liquid-to-air membrane energy exchanger (LAMEE) test facility development, commissioning and evaluating the steady-state performance, Energy Build. 66 (2013) 424–436, https://doi.org/10.1016/j.enbuild.2013.07.017.

[23] A. Datta, V. Rakesh, An Introduction to Modeling of Transport Processes, Cambridge University Press, The Edinburgh Building, Cambridge, 2010.

[24] P.M. Conde, Properties of aqueous solutions of lithium and calcium chlorides: formulations for use in air conditioning equipment design, Int. J. Therm. Sci. 43 (2004) 367–382, https://doi.org/10.1016/j.ijthermalsci.2003.09.003.

[25] C.J. Geankoplis, Transport Processes and Separation Process Principles (Includes Unit Operation), fourth ed., Prentice Hall International Inc, Upper Saddle River, 2003.

[26] L.Z. Zhang, Coupled heat and mass transfer in an application scale cross-flow hollow fiber membrane module for air humidification, Int. J. Heat Mass Transf. 55 (2012) 5861–5869, https://doi.org/10.1016/j.ijheatmasstransfer.2012.05.083.

[27] M.R.H. Abdel-Salam, R.W. Besant, C.J. Simonson, Sensitivity of the performance of a flat-plate liquid-to-air membrane energy exchanger (LAMEE) to the air and solution channel widths and flow maldistribution, Int. J. Heat Mass Transf. 84 (2015) 1082–1100, https://doi.org/10.1016/j.ijheatmasstransfer.2015.01.042.

[28] A. Fakharnezhad, P. Keshavarz, Experimental investigation of gas dehumidification by tri-ethylene glycol in hollow fiber membrane contactors, J. Ind. Eng. Chem. 34 (2016) 390–396, https://doi.org/10.1016/j.jiec.2015.12.021.

[29] S. Huang, M. Yang, X. Yang, Performance of a quasi-counter flow paralell-plate membrane contactor used for liquid desiccant air dehumidification, Appl. Therm. Eng. 63 (2014) 323–332, https://doi.org/10.1016/j.applthermaleng.2013.11.027.

[30] A.H. Abdel-Salam, C.J. Simonson, Annual evaluation of energy, environmental and economic performances of a membrane liquid desiccant air conditioning system with/without ERV, App. Energy 116 (2014) 134–148, https://doi.org/10.1016/j.apenergy.2013.11.047.

[31] G. Ge, D.G. Moghaddam, A.H. Abdel-Salam, R.W. Besant, C.J. Simonson, Comparison of experimental data and a model for heat and mass transfer performance of a liquid-to-air membrane energy exchanger (LAMEE) when used for air dehumidification and salt solution regeneration, Int. J. Heat Mass Transf. 68 (2014) 119–131, https://doi.org/10.1016/j.ijheatmasstransfer.2013.09.016.